



Cite this: *Phys. Chem. Chem. Phys.*,
2017, **19**, 27603

The role of Tat peptide self-aggregation in membrane pore stabilization: insights from a computational study†

Muhammad Jan Akhunzada,^a Balasubramanian Chandramouli,[‡]^a
Nicholus Bhattacharjee,^a Sara Macchi,[‡]^b Francesco Cardarelli,[‡]^b and
Giuseppe Brancato[‡]^{*ac}

It is widely accepted that endocytosis mediates the uptake of cationic cell penetrating peptides (CPPs) at relatively low concentrations (*i.e.* nano- to micromolar), while direct transduction across the plasma membrane comes into play at higher concentrations (*i.e.* micro- to millimolar). This latter process appears to depend on peptide-driven cellular processes, which in turn may induce local perturbations of plasma-membrane composition and/or integrity, and to be favored by peptide aggregation, especially into dimers. Besides, in most studies CPPs are tethered to fluorescent dyes in order to track peptide transduction events under the microscope, although often overlooking the possible role played by the dyes in assisting translocation. In an effort to provide some insights into the transduction process, here we report on a molecular dynamics (MD) simulation study of a prototype of the CPP family, namely the Tat₁₁ arginine-rich motif. To be specific, the translocation of Tat₁₁ across a purposely-created membrane pore, either or not covalently-linked to the tetramethylrhodamine-5-maleimide (TAMRA) dye and in both its monomeric and dimeric form, is analyzed in some detail. Results from several unconstrained and steered MD simulations, as well as energy decomposition analysis, nicely support the latest experimental evidence and help to shed light on key factors enabling peptide transduction. In particular, our study highlights the much slower translocation kinetics of Tat₁₁ dimer in comparison to the single peptide, and therefore its enhanced capability to stabilize membrane pores. Notably, it also shows how TAMRA has overall negligible kinetic and energetic effects on peptide transduction, yet it promotes this process indirectly by favoring peptide aggregation.

Received 27th July 2017,
Accepted 28th September 2017

DOI: 10.1039/c7cp05103d

rsc.li/pccp

1. Introduction

In the last three decades, intense research has been devoted to the investigation of the cellular uptake mechanism of cell penetrating peptides (CPPs), as they represent a promising platform for engineering safe and efficient drug delivery vectors (for more details, see exhaustive reviews ref. 1–4). It is now widely accepted that, among many factors, peptide concentration plays a key role in defining the specific route taken by the CPP to enter cells.⁵ More in detail, at relatively low CPPs concentrations, *i.e.* in the nanomolar to low-micromolar range, endocytosis is

the dominant mechanism.^{6–12} It has been shown that CPPs exploit distinct endocytic routes, such as macropinocytosis,⁴ clathrin-mediated endocytosis,¹³ and caveolae/lipid-raft-mediated endocytosis,^{14,15} depending on the exact peptide sequence tested, the nature of the attached cargo, the specific cell line used, *etc.* On the other hand, at higher CPPs concentrations, *i.e.* above 10 μM , spontaneous massive transduction across the plasma membrane becomes evident for most of the sequences studied so far. This uptake process leads to a rapid release of the peptide in the cell cytoplasm by maintaining the full integrity of the plasma membrane.² It is well known that CPPs transduction occurs across spatially confined regions of the plasma membrane, also known as nucleation zones (NZs)² (an experiment reproduced also here and reported in ESI,† Fig. S1). The exact nature of NZs has been extensively researched. It was shown, for instance, that cell-surface heparan sulphates (HS) on the plasma membrane are necessary for cytosolic transduction through NZs.⁵ Also, it was proposed that CPPs effective transduction involves peptide-driven activation of intracellular acid sphingomyelinase (ASMase),

^a Scuola Normale Superiore, piazza dei Cavalieri 7, I-56126 Pisa, Italy.

E-mail: giuseppe.brancato@sns.it

^b NEST, Scuola Normale Superiore and Istituto Nanoscienze-CNR, Piazza San Silvestro 12, 56127 Pisa, Italy

^c Istituto Nazionale di Fisica Nucleare, Largo Pontecorvo 3, I-56100 Pisa, Italy

† Electronic supplementary information (ESI) available. See DOI: 10.1039/c7cp05103d

‡ Present address: Compunet, Istituto Italiano di Tecnologia (IIT), Via Morego 30, I-16163 Genova, Italy.

followed by ceramide accumulation on the plasma membrane, local perturbation of membrane organization, and subsequent occurrence of peptide transduction at the border between ceramide-enriched regions and more fluid membrane domains.^{13,14} At the same time, experimental evidence of CPPs transduction across artificial membrane models, *i.e.* giant unilamellar vesicles (GUVs) and large unilamellar vesicles (LUVs),^{15–17} suggested that this process can happen also in absence of the complex cellular environment (see, *e.g.*, ref. 18). Of particular note, some of us recently proposed that an additional level of regulation, not directly related to the membrane, might be imparted by the peptide aggregation state.¹⁹ Briefly, it was shown that the Tat₁₁ arginine-rich peptide from HIV-1 Tat protein (sequence: **YGRKKRRQRRR**), which is the prototype of cationic CPPs, is able to self-aggregate in both its fluorescently labeled and unlabeled variants, exactly within the concentration range at which the shift in uptake mechanism (from endocytosis to transduction) is observed. Based on UV-Vis spectroscopy, NMR analysis and molecular dynamics (MD) simulations, Tat₁₁ dimerization was proposed as the dominant aggregation process, with an associated equilibrium constant increasing ten-folds by labeling with the standard TAMRA dye. Overall, these findings suggest that Tat₁₁ dimerization could play a role in facilitating transduction across the plasma membrane. This, in turn, is in keeping with several experimental observations using rationally engineered dimers/aggregates of Tat₁₁^{20–25} or related CPPs^{26–28} (obtained by covalent bonding or lysine linkage at the C-termini) showing enhanced cellular activity. Yet, the possible mechanistic relationship between Tat₁₁ self-dimerization and enhanced membrane transduction remains greatly elusive. However, the observation of NZs at high CPPs concentration may suggest the formation of local transitory structure in the plasma membrane. A plausible hypothesis could be that Tat₁₁ self-assembly does stabilize membrane pores, thus favoring the onset of a sustained membrane transduction process. A further issue concerns the assessment of the role of organic fluorescent dyes tethered to the CPPs. Fluorescent dyes are commonly used in imaging and molecular detection studies, for their capability to track molecules and to report on local polarity²⁹ or viscosity³⁰ in various environments.^{31–33} However, recent experimental evidence highlighted a possible non-neutral role for dye labeling in assisting CPP translocation.^{19,34}

In an effort to shed some light on these issues, which might have tremendous implications for the development of new therapeutic approaches, we present a computational study on the role of Tat₁₁ self-aggregation in membrane pore stabilization. In view of the experimental results mentioned above, we have taken into consideration both the native and the TAMRA-labeled Tat₁₁ peptide and we have carried out a kinetic analysis of the peptide in its monomeric and dimeric forms inside a purposely-created membrane pore, through extensive MD simulations. Therefore, the main goal of the present study is to evaluate the capability of the peptide to stabilize a lipid membrane pore over a prolonged period of time. In particular, we have extended the CHARMM force field for the treatment of the covalently linked TAMRA dye and performed both standard and steered MD simulations to characterize peptide escape-route kinetics.

Results nicely support experimental evidence and further corroborate the view of a special role played by CPP self-aggregation in membrane transduction. Besides, our study suggests an effective, though indirect, action of the TAMRA dye in favoring CPP translocation.

2. Material and methods

2.1 Model system generation

Tat₁₁ peptide is coupled with tetramethylrhodamine-5-maleimide (TAMRA, scheme depicted in Fig. 1) by addition of a cysteine residue at the C-terminal end. Both Tat₁₁ and dye-labeled Tat₁₁ (hereafter, referred to as Tat₁₁-TAMRA) were modeled according to the CHARMM36³⁵ force field, which is an additive, all-atom model that fixes some flaws in previous CHARMM27 and CHARMM27r force field resulting in greater accuracy. Topology of the TAMRA moiety was prepared using the model builder tools available in VMD³⁶ software. Bonded and non-bonded parameters were assigned by analogy to preexisting models of organic functional groups in the standard CHARMM force field. Atomic charges were obtained from a previous model¹⁹ and are reported in ESI,[†] Table S1. Initially, equilibrated configurations for Tat₁₁ and Tat₁₁-TAMRA peptide and for Tat₁₁-TAMRA dimer were obtained from a previous computational study.¹⁹ A pre-equilibrated hydrated bilayer made up of 400 1,2-dioleoyl-*sn*-glycero-3-phosphocholine (DOPC) lipids was used to generate the initial membrane pore system following the procedure described in Section 3.1. However, to speed up calculations, after pore formation and equilibration the lipid system was reduced to 320 DOPC molecules, without affecting the overall membrane stability. In this case, the CHARMM36³⁵ force field for lipids was used to model the membrane bilayer. The obtained membrane pore system was then used for all peptide translocation simulations reported in the study, by preliminarily introducing the peptide within the pore in a parallel configuration to the orthogonal axis of the lipid bilayer, as depicted in Fig. 2A and B. Chloride ions were added to ensure electric charge neutrality. All the systems were set up to run spontaneous, unconstrained MD simulations. Details on all simulated systems are collected in ESI,[†] Table S2.

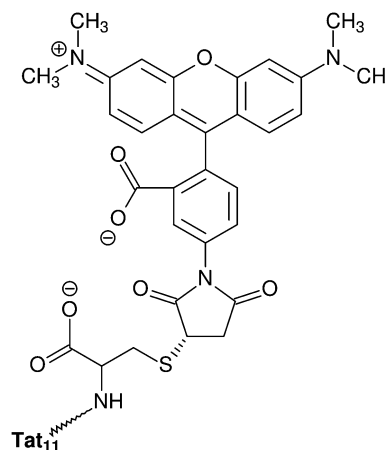


Fig. 1 Chemical structure of TAMRA dye covalently linked to the Tat₁₁ peptide.

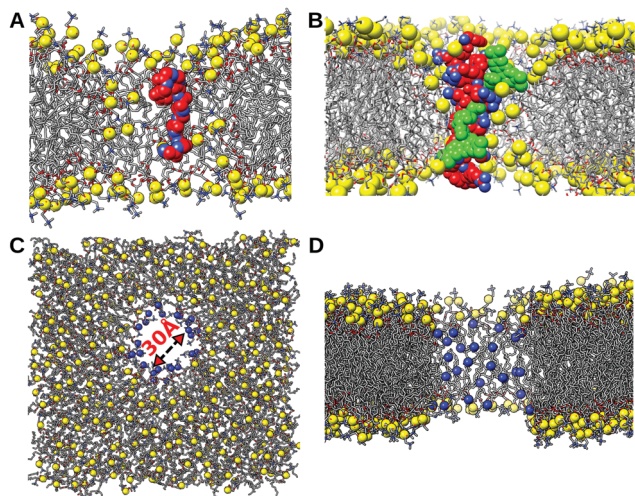


Fig. 2 Representative initial configurations of (A) Tat₁₁ and (B) Tat₁₁-TAMRA dimer peptides as embedded into a DOPC membrane pore. Peptide backbone is depicted in vdW representation, O atoms in red and N atoms in blue. Lipid chains are depicted in gray, phosphate groups in yellow. (C) Top and (D) side views of an equilibrated molecular configuration of the membrane pore. Lipid chains are depicted in gray, phosphate groups in yellow and lipid head groups shaping the pore in blue.

2.2 Molecular dynamics simulations

All MD simulations were performed under periodic boundary conditions using NAMD v2.10 software package.³⁷ The SHAKE algorithm³⁸ was adopted to keep all bonds containing hydrogen atoms rigid, with a time step of 2 fs. Long-range electrostatic interactions were computed using the particle mesh Ewald (PME)³⁹ method, while nonbonded interactions were evaluated with a cutoff radius of 12 Å, with a smoothing function applied at 10 Å. Constant pressure of 1 atm was enforced by using the Noose–Hover Langevin piston^{40,41} and Langevin dynamics was employed to keep the temperature constant at 303.15 K (30 °C) which is above the main phase transition temperature (−20 °C) for DOPC.^{42,43} In particular, a semi-isotropic *NpT* algorithm was imposed to allow the area of the lipid membrane (*i.e.*, *XY* plane) to change independently from its orthogonal axis (*i.e.*, *Z*-coordinate). All systems underwent a preliminary energy minimization and a short room-temperature MD equilibration. In particular, both monomer and dimer systems, once introduced into the lipid bilayer by aligning the peptide along the pore axis, were equilibrated for a few (about 5 ns) nanoseconds to slowly move the center of mass of the peptide to the bilayer center (*i.e.*, center of mass of phosphate groups). For each system, three production runs were carried out according to the *NpT* ensemble for some hundreds of nanoseconds (from 500 ns to 1 μs, see more details in ESI,† Table S2). In the literature, it was reported that complete translocation of CPPs across plasma membrane could take up to 1 ms.^{44,45} In our study, it was not possible to see the spontaneous translocation of the Tat₁₁-TAMRA dimer within the simulated time interval during unconstrained MD simulations. In this case, a convenient computational approach consists to rely on steered MD (SMD) simulations to induce translocation of molecules through pores and channels.⁴⁶

Hence, we also performed SMD simulations in order to pull the Tat₁₁-TAMRA monomer and dimer systems, while recording the pulling force required to drag the peptide across the membrane out into the bulk solution. SMD simulations (see ESI,† Table S2) allowed obtaining an average pulling force profile for peptide translocation. Center of mass of peptide and its aggregated form were pulled along the orthogonal axis (*i.e.*, *Z*-coordinate) of the bilayer according to a constant velocity (1 Å ns^{−1}) algorithm (*i.e.*, the pulling force is the force needed to pull the peptide along the pore while it translocates out of the membrane at constant velocity and it is recorded at each step during the SMD simulation, see NAMD³⁷ manual for more details). Four replica simulations with same pulling velocity were performed for both Tat₁₁-TAMRA monomer and dimer systems as reported in ESI,† Table S2. Besides, energetic and hydrogen bonding analyses of the systems considered here were performed with the VMD software (in this case, one MD trajectory for each system was analyzed), while other structural analysis were performed with in-house codes.

3. Results and discussion

3.1 Membrane pore formation and stabilization

Despite many experimental and theoretical studies have investigated pore formation in membranes, this process remains still not fully understood, especially in live cells. Whether CPPs have a promoting effect towards the appearance of pores in cellular and model lipid membranes it is still unclear. Different studies based on confocal microscopy and dye translocation seem to indicate that transient pore structures may determine the observed inward flux in NZs at high CPP concentration. Besides, from a computational point of view, it is highly unlikely the observation of spontaneous pore formation and translocation events on the typical timescales accessible to MD simulations.^{47,48} For the reasons sketched above and in analogy with previous studies,^{48,49} in this work we decided to artificially create a pore into a previously equilibrated DOPC lipid bilayer, then introducing a peptide monomer or dimer to carefully investigate its exit pathway dynamics. Starting from a pre-equilibrated 400 DOPC lipid bilayer, we sequentially applied an increasing surface tension from 40 to 90 dyn per cm in an isothermal–isobaric ensemble, over a simulation time interval of about 70 ns, in order to induce membrane rupture (*i.e.*, tension applied parallel to the membrane along the *XY* plane). During the simulation, a further water layer of about 24 Å was added owing to the excessive thinning of the membrane/water system. Once membrane rupture occurred, a number of pores formed rapidly and became well solvated, owing to the acquired bilayer instability. Among them, a pore of more than 20 Å of radius was obtained. Then, the lipid membrane was relaxed (*i.e.*, *NpT* ensemble) without any tension applied to restore its overall structure at normal conditions (*i.e.*, area per lipids and thickness). During this simulation step, spanning about 60 ns, the large pore previously observed was stabilized by applying positional restraints to the water molecules located into a

cylindrical region of 15 Å radius lined up across the lipid bilayer and with the axis center taken approximately in the middle of the pore. Note that all other pores sealed back during this equilibration step. Under such conditions, a well-formed membrane pore was equilibrated within the lipid bilayer (Fig. 2C and D), hence preventing its closure (*i.e.*, final equilibrated pore was 30 Å width and about 40 Å long). Overall, structural parameters of the membrane, such as lipid density (area per lipid: $69.4 \pm 0.6 \text{ \AA}^2$) and thickness ($39.0 \pm 0.6 \text{ \AA}$), evaluated by excluding the pore region, nicely reproduced those of the native lipid bilayer (area per lipid: $68.2 \pm 0.6 \text{ \AA}^2$; membrane thickness: $38.5 \pm 0.4 \text{ \AA}$).

3.2 Tat₁₁ and Tat₁₁-TAMRA peptide translocation

As a first step in our kinetics study, we have located a Tat₁₁ and Tat₁₁-TAMRA peptide inside the pre-formed membrane defect (*i.e.* pore). After introduction of the peptide into the pore, a short equilibration run was carried out to bring the center of mass of the peptide to the center of mass of the lipid membrane and to equilibrate the peptide within this confinement. Hence, unconstrained MD simulations of both peptide monomers have been carried out for several hundreds of nanoseconds in a *NpT* ensemble. To gain more statistics, we carried out multiple simulations for each peptide, for a total of six extended MD simulations (see details in Section 2 and ESI,† Table S2). The interaction energy between the Tat₁₁ peptide (and its labeled variant) and lipids was computed from the simulated trajectories by selecting an initial time interval of about 100 ns displaying the peptide buried inside the lipid bilayer (Table 1). To better characterize such an interaction and to evaluate possible differences due to the presence of the dye, the interaction energy was decomposed in Coulomb and van der Waals terms. In addition, the distinct contributions of TAMRA and arginine residues were also considered. As shown in Table 1, the interaction between the Tat₁₁ peptide with the phospholipids inside the pore is dominated by electrostatics owing to the electrically charged peptide residues (*i.e.*, Arg), with other interaction terms having a minor role. Indeed, the contribution of arginine residues interacting with the phospholipid head groups basically account for the interaction of Tat₁₁. Moreover, no significant energy difference exists between the labeled and unlabeled peptide taking into account statistical noise, TAMRA dye adding negligible effects on overall interaction. Tat₁₁ and Tat₁₁-TAMRA also showed a similar hydrogen bonding pattern, both peptides forming, on average, about six hydrogen bonds with surrounding lipids.

To proceed further, we have inspected Tat₁₁ peptide dynamics in all systems under study. In one notable case, Tat₁₁ monomer underwent full translocation out from the lipid membrane in about 450 ns, as shown in Fig. 3A and B. In other two parallel simulations carried out for up to 400 ns, the same peptide has shown significant movements towards bulk solution though not completely out of the pore (ESI,† Fig. S2). Similarly, Tat₁₁-TAMRA was able to move out of the pore in two simulations after about 300 ns and 550 ns (Fig. 3C, D and ESI,† Fig. S3), whereas in a third case a complete translocation could not be observed, as shown in ESI,† Fig. S3. Overall, our results show that, once inserted into a lipid pore membrane, Tat₁₁ peptide has a translocation time in the sub- to 1-microsecond timescale, even if the poor statistics does not allow us to estimate it exactly. This timescale also reflects into the lifetime of the membrane defect before sealing back, which is substantially extended in this case (*i.e.*, about one order of magnitude) with respect to the observed pore re-closure, as revealed by a test simulation in the absence of any peptide (*i.e.*, about 30 ns). These findings are well in line with previous studies^{48,49} reporting, for example, a comparable kinetics for the Arg₈ homopeptide, whereas the Lys₈ homopeptide apparently showed a fast translocation due to significantly weaker interactions with the lipids.

3.3 Tat₁₁-TAMRA monomer versus dimer translocation

By a combination of cell uptake, NMR, UV-Vis and MD study,¹⁹ some of the authors have already shown that Tat₁₁ and Tat₁₁-TAMRA do form dimeric structures in solution at high concentration (*i.e.* micro- to millimolar). In particular, Tat₁₁-TAMRA does form prevalently dimers above the 5–10 μM threshold, whereas the unlabeled peptide shows self-aggregation at much higher concentration (>150 μM). Interestingly, above their corresponding threshold, both Tat₁₁ peptides show a marked change of cell uptake mechanism, from energy-dependent endocytosis to diffusive peptide transduction. Here, we set out to probe the capability of Tat₁₁-TAMRA, in its dimeric form, to kinetically stabilize the membrane defect with respect to the corresponding monomeric unit. To this end, following the same protocol described above, the equilibrated structure of a transient Tat₁₁-TAMRA dimer was introduced into the pore of the lipid bilayer and initially equilibrated by restraining its longitudinal motions along the pore axis (*i.e.*, an harmonic potential was applied to the dimer center of mass). Afterwards, all restraints were released, the system was replicated two times with initial velocities randomly regenerated and three fully unconstrained MD simulations were carried out. All Tat₁₁-TAMRA dimer systems

Table 1 Interaction energy and H-bond analysis of Tat₁₁ and Tat₁₁-TAMRA peptides with DOPC

Int. energy	Tat ₁₁ /lipid	Tat ₁₁ -T/lipid	(Tat ₁₁ -T) ₂ /lip.	Arg/lip. head	Lys/lip. head	T/lip. head
Coulomb	−1120	−1035	−1913	−1309	−610	31
vdW	−87	−103	−191	−4	−8	−8
Total	−1207 ± 130	−1138 ± 130	−2104 ± 230	−1313 ± 160	−618 ± 152	23 ± 20
H-Bonds	6.2	6.4	10.7	4.6	1.3	0

Tat₁₁: Tat₁₁ monomer; Tat₁₁-T: Tat₁₁-TAMRA monomer; (Tat₁₁-T)₂: Tat₁₁-TAMRA dimer; T: TAMRA; Arg: arginine; Lys: lysine. Units are in kcal mol^{−1}. Interaction energy and H-bond analyses were performed on an initial time interval of the MD trajectories (100 ns).

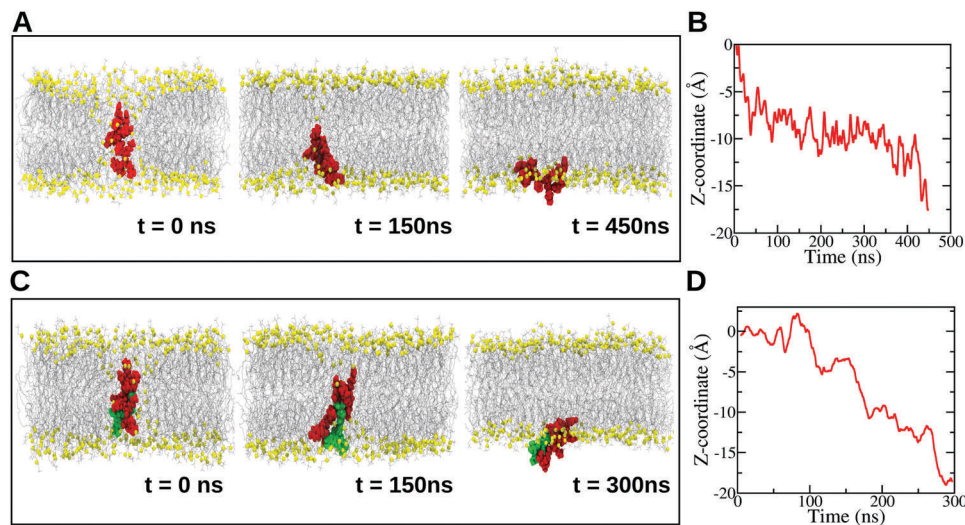


Fig. 3 Snapshot configurations issuing from (A) Tat₁₁ and (C) Tat₁₁-TAMRA MD simulations taken at different time intervals. Peptides are depicted in red with TAMRA dye in green. (B–D) Corresponding translocation distance of monomer center of mass along the longitudinal pore axis (*i.e.*, Z-coordinate, see Section 2.2 for details).

showed significant resistant to move along the pore and, as a consequence, no one exited from the pore despite simulation was extended up to 1 microsecond, as shown in Fig. 4 and ESI,† Fig. S4. Besides, no noticeable peptide conformational changes were observed. Therefore, Tat₁₁ peptide in its aggregated form, with twice the number of arginine residues (*i.e.*, 12 Arg), has shown a translocation kinetics in stark contrast to its monomeric counterpart: the physical origin of the slower kinetics is ascribed to both the higher inertial mass and the stronger interaction of Tat₁₁-TAMRA dimer with the lipids lining the pore. To further confirm, we evaluated the interaction energy of the dimer with the surrounding lipids and compared results to the ones for the individual peptide. Results are reported in Table 1 highlighting the enhanced interaction (about twice the interaction energy and the number of hydrogen bonds) of the self-assembled peptide with respect to the monomer, with a predominant contribution from electrostatics. Indeed, strong binding between the peptide and the lipids lining the pore is the reason that prevents lipid reorganization and pore sealing.^{47,48} Beside, we noticed that lysine residues have little interaction with the surrounding lipids (see Fig. S5, ESI†), the average number of hydrogen bonds being 1.3 and the interaction energy between lysine residues and lipid heads being

less than half of the one for arginine residues (Table 1). Note also that there are two Lys residues per peptide monomer.

Furthermore, due to the limits of the timescales typically accessible to atomistic simulations, we relied upon steered molecular dynamics (SMD) to make a more direct comparison between the Tat₁₁-TAMRA monomer and dimer system. To this purpose, SMD simulations were carried out by gently pulling the center of mass of each peptide system initially centered within the lipid bilayer, along the longitudinal axis (*i.e.*, Z-coordinate) of the pore and at constant velocity (*i.e.*, 1 Å ns⁻¹) towards bulk solution (Fig. 5). All simulations were carried out for about 40 ns, recording the pulling force required to drive the peptide out every 1 ps. The pulling forces were then averaged in bins of 2 Å width along the Z-coordinate representing the distance from the center of the pore and then averaged over all four simulated trajectories (see details in ESI,† Table S2). The resulting pulling force as a function of distance for both dye-labeled Tat₁₁ monomer and dimer are depicted in Fig. 6. At the beginning, it can be clearly observed that the force to pull the two peptide systems out of the pore is gradually increasing in a similar fashion, up to about 15 Å. At this point, however, a stark divergent profile becomes apparent with the force for dragging the dimeric form notably higher than the one needed

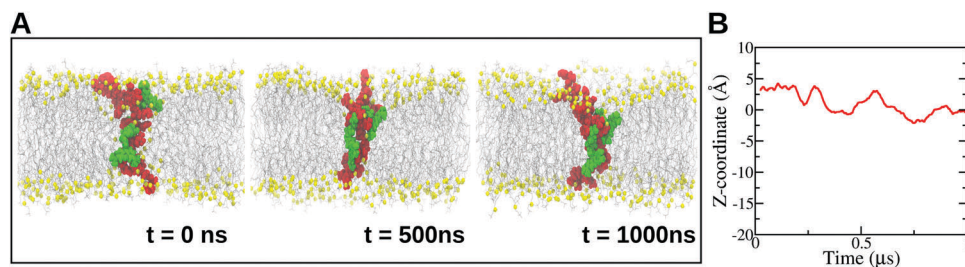


Fig. 4 (A) Snapshot configurations issuing from Tat₁₁-TAMRA dimer MD simulation taken at different time intervals. Peptides are depicted in red with TAMRA dye in green. (B) Corresponding translocation distance of dimer center of mass along the longitudinal pore axis (*i.e.*, Z-coordinate).

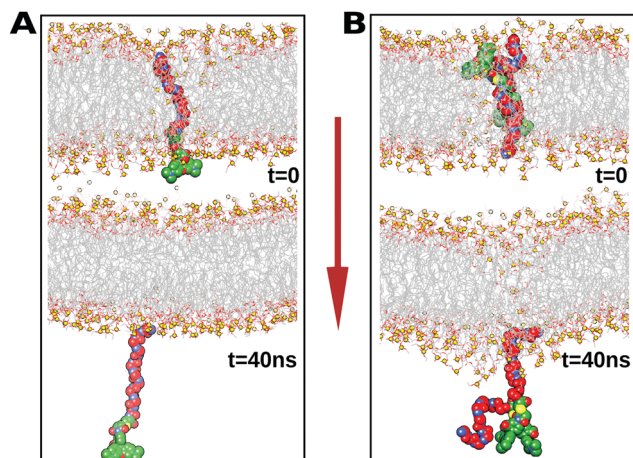


Fig. 5 Initial (top) and final (after 40 ns, bottom) configurations issuing from Tat₁₁-TAMRA (A) monomer and (B) dimer SMD simulations. Peptide are depicted in red with TAMRA dye in green. Red arrow shows the direction of applied pulling force along the longitudinal pore axis (*i.e.*, Z-coordinate).

for the monomer. Maximum value of pulling force reached about 150 pN, in the case of the monomer, and well above 220 pN, in the case of the dimer (max. difference between the two systems was > 100 pN). At longer distances, the two force profiles declined and then converged again toward the end, at about 35 Å. Overall, Tat₁₁-TAMRA dimer required a larger pulling force to be completely extracted from within the lipid bilayer, thus supporting a higher kinetic energy barrier than its monomeric counterpart. This finding is in good agreement with our previous unconstrained MD simulations and energy analysis. Note also that peptide structures are not significantly distorted throughout the SMD simulations with respect to their corresponding initial configuration.

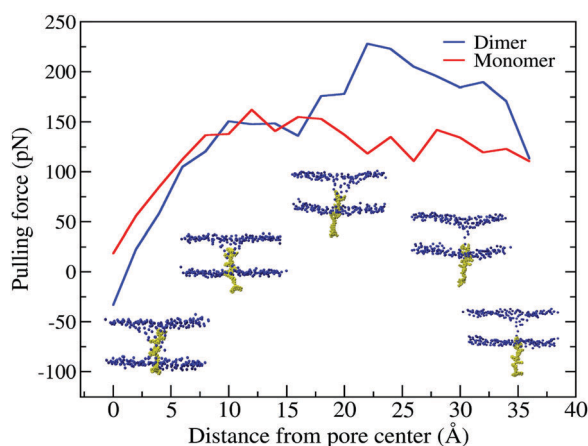


Fig. 6 Average pulling force applied to gently move the Tat₁₁-TAMRA peptide (both monomeric and dimeric forms) out of the membrane pore as a function of distance from the lipid bilayer center. The resulting force profile is evaluated as the average of four SMD simulations for each system under consideration. Peptide (yellow) at various distances from pore center is depicted in the insets, with lipid head groups in blue. Standard error is 25 pN.

We may argue that the ability to inhibit pore closure can be crucial in the stabilization of membrane defects by Tat₁₁ when used at high concentrations, independently on the exact origin of the membrane defect. Of note, similar evidences were so far reported on selected variants of Tat₁₁ peptide. First, some of us recently showed by MD simulations that a pore-like membrane defect can be similarly stabilized by Tat₁₁ fused to CM₁₈,⁵⁰ an antimicrobial peptide capable of enhancing Tat₁₁ membrane disruption capabilities through carpet-like detergent effects.^{51–53} Also, the higher pore-stabilization capability of the Tat₁₁ dimer observed here agrees well with previous experimental reports showing that membrane transduction is greatly favored by the rational engineering of Tat₁₁ dimers. In particular, it was reported that Tat₁₁ dimers obtained by covalent bonds or Lysine linkage at the C-termini show enhanced cellular activity in terms of uptake efficacy and membrane destabilization.^{20–25} Of particular note is the work by Erazo-Oliveras *et al.*²¹ reporting on an engineered tetramethylrhodamine-labeled Tat dimer, closely resembles the self-assembled dimer investigated in our study, which is able to mediate efficient endosomal leakage and deliver exogenous proteins into cultured cells after a simple co-incubation procedure.²¹ Moreover, we note that arginine has the ability to make bidentate hydrogen bonds with multiple phosphate moieties on the lipid head groups, thus favoring peptide adsorption on the membrane surface, pore stabilization and, ultimately, peptide transduction.⁵⁴ The number of arginine residues present in a peptide chain could be the determining factor in the process of direct transduction, with the optimum number leading to more efficient translocation between 6 to 12 Arg, while more than 16 arginine residues in a peptide showed little or no transduction capabilities.^{55,56} This is consistent with our results from spontaneous and SMD simulations as Tat₁₁ dimer has twice the number of arginine residues and, as a consequence, the overall energy required to break the bonds between arginine and neighboring phosphates is higher in aggregated Tat₁₁.

3.4 TAMRA dye: spectator or active role?

Most of the literature reporting on CPP cell-entry mechanisms entails the use of organic fluorophores for real-time tracing of peptide localization and activity, often without questioning on the possible effects brought about by such dyes. In this view, any gain of knowledge on the role of dye labeling on peptide uptake by cells or vesicles can help to rationalize previous observations and possibly guide new strategies of peptide engineering. Worthy of note, in our study we have observed no significant effect of the standard TAMRA dye both on the interaction energy of Tat₁₁ monomer with membrane lipids and on the peptide residence time within the pore. This may suggest for TAMRA dye the role of a neutral watcher during Tat₁₁-pore interaction. On the other hand, however, we know from previous MD, NMR and UV-Vis analyses that TAMRA dye plays instead an active role in mediating monomer-monomer interactions, thus greatly favoring peptide aggregation as compare to unlabeled species.¹⁹ Moreover, previous experimental studies, here fully confirmed by our *in silico* investigation, have

suggested the special role of CPP dimers in penetrating plasma membranes and stabilizing membrane defects, then leading to the possible formation of NZs. Combined together, these results draw a final picture in which the TAMRA dye can be seen as a critical actor in the process of Tat₁₁ membrane transduction: it promotes peptide dimerization and, by doing this, it remarkably slows down the translocation kinetics, thus enhancing, at the same time, the lifetime of the defect.

4. Conclusions

In this *in silico* study, we provided some further insights on a very complex and challenging cellular process, namely CPPs direct transduction through plasma membranes, whose action mechanism and efficacy have far-reaching consequences for understanding cell biophysics and for therapeutic developments. Remarkable differences have been uncovered between Tat₁₁ peptide in its monomeric and dimeric forms. For the purposes of the study, a lipid bilayer pore was preliminarily created to investigate specifically the translocation kinetics of the CPP once inserted into the pore and the interactions with the surrounding lipids at molecular level. The much slower kinetics of the Tat₁₁ aggregated form with respect to the monomeric counterpart, as observed in our simulations, was rationalized in terms of the higher interaction energy and hydrogen bondings between the peptide and the lipids shaping the translocation pore, in addition to the larger inertial mass. Tat₁₁ dimer, which has double the number of arginine residues than the monomer, was able to stabilize the membrane pore over a prolonged period of time (>1 μ s). Such an enhanced pore stabilization effect by the Tat₁₁ dimer is attributed to the strong Coulomb interactions between arginine residues and surrounding lipid head groups. It was also proved further with the help of our SMD simulations that the force required to pull the dimer out of the pore by breaking up such electrostatic interactions was significantly larger (*i.e.*, $\times 2$) than in the case of the monomer. Such interactions then interrupt the process of lipid diffusion required by the pore to close back and significantly extend the membrane defect lifetime (we may predict the difference to be a few orders of magnitude). Notably, results on the Tat₁₁-TAMRA peptide have also helped to assess the role of dye labeling in the translocation process of CPPs. In this case, our findings, coupled with previous experimental evidence, allow us to propose for TAMRA a “supporting actor” role towards peptide transduction, the dye being able to promote effectively self-aggregation at micromolar concentration, though not adding any relevant contribution to lipid interaction. Whether the present conclusions could be also extended to other dyes of widespread use in CPP translocation studies is a question that calls for further verifications. It is worth noting that in our comparative study lipid composition, which is an important factor possibly influencing peptide transduction, was not taken into examination. However, since our focus was on the effects of self-aggregation and dye tethering, the overall picture emerging from our results is expected to remain substantially

unaltered for a number of lipids and lipid mixtures. We believe our work may provide supportive ideas to peptide design and engineering in a large number of targeted applications aiming at improving CPP-mediated delivery inside the cells.

Conflicts of interest

There are no conflicts to declare.

Acknowledgements

G.B. acknowledges the financial support of the INFN, the Scuola Normale Superiore research program and the FAS Salute Regione Toscana Project “DIAMANTE”. We thank Dr Riccardo Nifosi for useful discussions and for providing initial structures of the Tat₁₁ and Tat₁₁-TAMRA peptides.

References

- 1 C. Bechara and S. Sagan, *FEBS Lett.*, 2013, **587**, 1693–1702.
- 2 R. Brock, *Bioconjugate Chem.*, 2014, **25**, 863–868.
- 3 A. T. Jones and E. J. Sayers, *J. Controlled Release*, 2012, **161**, 582–591.
- 4 T. Takeuchi and S. Futaki, *Chem. Pharm. Bull.*, 2016, **64**, 1431–1437.
- 5 F. Duchardt, M. Fotin-Mleczek, H. Schwarz, R. Fischer and R. Brock, *Traffic*, 2007, **8**, 848–866.
- 6 K. Cleal, L. He, P. D. Watson and A. T. Jones, *Curr. Pharm. Des.*, 2013, **19**, 2878–2894.
- 7 S. El-Andaloussi, H. J. Johansson, P. Lundberg and Ü. Langel, *J. Gene Med.*, 2006, **8**, 1262–1273.
- 8 A. Fittipaldi, A. Ferrari, M. Zoppé, C. Arcangeli, V. Pellegrini, F. Beltram and M. Giacca, *J. Biol. Chem.*, 2003, **278**, 34141–34149.
- 9 I. M. Kaplan, J. S. Wadia and S. F. Dowdy, *J. Controlled Release*, 2005, **102**, 247–253.
- 10 I. Nakase, M. Niwa, T. Takeuchi, K. Sonomura, N. Kawabata, Y. Koike, M. Takehashi, S. Tanaka, K. Ueda, J. C. Simpson, A. T. Jones, Y. Sugiura and S. Futaki, *Mol. Ther.*, 2004, **10**, 1011–1022.
- 11 J. P. Richard, K. Melikov, H. Brooks, P. Prevot, B. Lebleu and L. V. Chernomordik, *J. Biol. Chem.*, 2005, **280**, 15300–15306.
- 12 P. Säälilik, A. Elmquist, M. Hansen, K. Padari, K. Saar, K. Viht, Ü. Langel and M. Pooga, *Bioconjugate Chem.*, 2004, **15**, 1246–1253.
- 13 W. P. R. Verdurmen, M. Thanos, I. R. Ruttekkolk, E. Gulbins and R. Brock, *J. Controlled Release*, 2010, **147**, 171–179.
- 14 F. M. Goñi and A. Alonso, *FEBS Lett.*, 2002, **531**, 38–46.
- 15 A. Lamazière, F. Burlina, C. Wolf, G. Chassaing, G. Trugnan and J. Ayala-Sanmartin, *PLoS One*, 2007, **2**, e201.
- 16 D. Persson, P. E. G. Thorén, E. K. Esbjörner, M. Goksör, P. Lincoln and B. Nordén, *Biochim. Biophys. Acta, Biomembr.*, 2004, **1665**, 142–155.
- 17 J.-M. Swiecicki, A. Bartsch, J. Tailhades, M. Di Pisa, B. Heller, G. Chassaing, C. Mansuy, F. Burlina and S. Lavielle, *ChemBioChem*, 2014, **15**, 884–891.

- 18 M. Di Pisa, G. Chassaing and J.-M. Swiecicki, *Biochemistry*, 2015, **54**, 194–207.
- 19 S. Macchi, R. Nifosi, G. Signore, S. Di Pietro, C. Boccardi, F. D'Autilia, F. Beltram and F. Cardarelli, *Phys. Chem. Chem. Phys.*, 2017, **19**, 23910–23914.
- 20 A. Chugh and F. Eudes, *Biochim. Biophys. Acta, Biomembr.*, 2007, **1768**, 419–426.
- 21 A. Erazo-Oliveras, K. Najjar, L. Dayani, T.-Y. Wang, G. A. Johnson and J.-P. Pellois, *Nat. Methods*, 2014, **11**, 861–867.
- 22 J. T. Pepper, P. Maheshwari and F. Eudes, *Colloids Surf., B*, 2017, **157**, 207–214.
- 23 C. Rudolph, U. Schillinger, A. Ortiz, K. Tabatt, C. Plank, R. H. Müller and J. Rosenecker, *Pharm. Res.*, 2004, **21**, 1662–1669.
- 24 I. A. Monreal, Q. Liu, K. Tyson, T. Bland, D. S. Dalisay, E. V. Adams, G. A. Wayman, H. C. Aguilar and J. P. Saludes, *Chem. Commun.*, 2015, **51**, 5463–5466.
- 25 A. Jain, S. G. Shah and A. Chugh, *Pharm. Res.*, 2015, **32**, 1920–1930.
- 26 J. A. Moss, A. Lillo, Y. S. Kim, C. Gao, H. Ditzel and K. D. Janda, *J. Am. Chem. Soc.*, 2005, **127**, 538–539.
- 27 J. Hoyer, U. Schatzschneider, M. Schulz-Siegmund and I. Neundorff, *Beilstein J. Org. Chem.*, 2012, **8**, 1788–1797.
- 28 S. Macchi, G. Signore, C. Boccardi, C. D. Rienzo, F. Beltram and F. Cardarelli, *Sci. Rep.*, 2015, **5**, 16914.
- 29 G. Brancato, G. Signore, P. Neyroz, D. Polli, G. Cerullo, G. Abbandonato, L. Nucara, V. Barone, F. Beltram and R. Bizzarri, *J. Phys. Chem. B*, 2015, **119**, 6144–6154.
- 30 M. Koenig, G. Bottari, G. Brancato, V. Barone, D. M. Guldi and T. Torres, *Chem. Sci.*, 2013, **4**, 2502.
- 31 M. Koenig, B. Storti, R. Bizzarri, D. M. Guldi, G. Brancato and G. Bottari, *J. Mater. Chem. C*, 2016, **4**, 3018–3027.
- 32 M. Koenig, T. Torres, V. Barone, G. Brancato, D. M. Guldi and G. Bottari, *Chem. Commun.*, 2014, **50**, 12955–12958.
- 33 P. Minei, M. Koenig, A. Battisti, M. Ahmad, V. Barone, T. Torres, D. M. Guldi, G. Brancato, G. Bottari and A. Pucci, *J. Mater. Chem. C*, 2014, **2**, 9224–9232.
- 34 M. G. Di Carlo, V. Minicozzi, V. Foderà, V. Militello, V. Vetri, S. Morante and M. Leone, *Biophys. Chem.*, 2015, **206**, 1–11.
- 35 J. B. Klauda, R. M. Venable, J. A. Freites, J. W. O'Connor, D. J. Tobias, C. Mondragon-Ramirez, I. Vorobyov, A. D. MacKerell and R. W. Pastor, *J. Phys. Chem. B*, 2010, **114**, 7830–7843.
- 36 W. Humphrey, A. Dalke and K. Schulten, *J. Mol. Graphics*, 1996, **14**, 33–38.
- 37 J. C. Phillips, R. Braun, W. Wang, J. Gumbart, E. Tajkhorshid, E. Villa, C. Chipot, R. D. Skeel, L. Kalé and K. Schulten, *J. Comput. Chem.*, 2005, **26**, 1781–1802.
- 38 J.-P. Ryckaert, G. Ciccotti and H. J. C. Berendsen, *J. Comput. Phys.*, 1977, **23**, 327–341.
- 39 T. Darden, D. York and L. Pedersen, *J. Chem. Phys.*, 1993, **98**, 10089–10092.
- 40 S. E. Feller, Y. Zhang, R. W. Pastor and B. R. Brooks, *J. Chem. Phys.*, 1995, **103**, 4613–4621.
- 41 G. J. Martyna, D. J. Tobias and M. L. Klein, *J. Chem. Phys.*, 1994, **101**, 4177–4189.
- 42 G. R. Kneller, K. Baczynski and M. Pasenkiewicz-Gierula, *J. Chem. Phys.*, 2011, **135**, 141105.
- 43 N. Kučerka, S. Tristram-Nagle and J. F. Nagle, *J. Membr. Biol.*, 2006, **208**, 193–202.
- 44 H. D. Hecce, A. E. Garcia, J. Litt, R. S. Kane, P. Martin, N. Enrique, A. Rebolledo and V. Milesi, *Biophys. J.*, 2009, **97**, 1917–1925.
- 45 S. Yesylevskyy, S.-J. Marrink and A. E. Mark, *Biophys. J.*, 2009, **97**, 40–49.
- 46 B. Chandramouli, D. Di Maio, G. Mancini and G. Brancato, *Biochim. Biophys. Acta, Biomembr.*, 2016, **1858**, 689–697.
- 47 K. Akabori, K. Huang, B. W. Treece, M. S. Jablin, B. Maranville, A. Woll, J. F. Nagle, A. E. Garcia and S. Tristram-Nagle, *Biochim. Biophys. Acta, Biomembr.*, 2014, **1838**, 3078–3087.
- 48 D. Sun, J. Forsman and C. E. Woodward, *J. Phys. Chem. B*, 2015, **119**, 14413–14420.
- 49 D. Sun, J. Forsman, M. Lund and C. E. Woodward, *Phys. Chem. Chem. Phys.*, 2014, **16**, 20785–20795.
- 50 F. Salomone, M. Breton, I. Leray, F. Cardarelli, C. Boccardi, D. Bonhenry, M. Tarek, L. M. Mir and F. Beltram, *Mol. Pharmaceutics*, 2014, **11**, 2466–2474.
- 51 A. Fasoli, F. Salomone, M. Benedusi, C. Boccardi, G. Rispoli, F. Beltram and F. Cardarelli, *Molecules*, 2014, **19**, 9228–9239.
- 52 F. Salomone, F. Cardarelli, M. Di Luca, C. Boccardi, R. Nifosi, G. Bardi, L. Di Bari, M. Serresi and F. Beltram, *J. Controlled Release*, 2012, **163**, 293–303.
- 53 F. Salomone, F. Cardarelli, G. Signore, C. Boccardi and F. Beltram, *PLoS One*, 2013, **8**, e70108.
- 54 A. Mishra, V. D. Gordon, L. Yang, R. Coridan and G. C. L. Wong, *Angew. Chem., Int. Ed.*, 2008, **47**, 2986–2989.
- 55 S. Futaki, T. Suzuki, W. Ohashi, T. Yagami, S. Tanaka, K. Ueda and Y. Sugiura, *J. Biol. Chem.*, 2001, **276**, 5836–5840.
- 56 N. Schmidt, A. Mishra, G. H. Lai and G. C. L. Wong, *FEBS Lett.*, 2010, **584**, 1806–1813.